Real-time noise reduction for sonar video image using recursive filtering

Hyeonwoo Cho, Juhyun Pyo, Jeonghwe Gu, Hangil Jeo, and Son-Cheol Yu
Department of Creative IT Engineering
Pohang University of Science and Technology
Pohang, Gyeongbuk, South Korea 37673
Email: lighto@postech.ac.kr

***Abstract*—The forward-looking imaging sonar is a prospective solution for underwater visual surveying because it allows long-range visibility in turbid water, and provides a high frame rate. However, the acoustic images are degraded by speckle noise. In this paper, we propose an algorithm to reduce the noise in a series of acoustic image frames obtained by using a forward-looking imaging sonar. The time-series model of the acoustic images are developed for predicting the changes in pixel coordinates. Also, the Kalman filter estimates the noise-reduced pixels of the images based on the acoustic image model. This recursive treatment is suitable for the successive image frames.**

I. Introduction

Underwater surveying is performed for various purposes, such as scientific research, maintenance of artificial structures, and investigations of underwater resource [1]. Although optical imaging, which is the primary method of ground surveying, can be applied for underwater surveying, the visibility of the optical image suffers underwater because of the back scattering and attenuation of visible light, as well as the turbidity of water [2], [3]. In contrast, acoustic imaging allows long-range visibility even though water is turbid. Therefore, acoustic imaging is a prospective solution for underwater surveying [4].

However, the quality of an acoustic image is lower than that of an optical image [5]. In particular, the acoustic image is degraded by speckle noise, which is multiplicative noise that appears in most acoustic images [6], [7]. To solve the problem of the speckle noise, adaptive filtering and wavelet filtering algorithms have been adopted [8], [9]. These algorithms focus on one acoustic image frame obtained using side-scan sonar that scans wide underwater areas. On the other hand, the forward-looking imaging sonar provides a series of acoustic images with high frame rate similar to that of an optical video camera [10], [11].

Generally, the noise of any time-varying signal can be eliminated by recursively averaging the signal [12]. Therefore the noise of pixels of successive acoustic images can be removed by averaging each pixel of the images over time. However, this strategy is only viable when there is no movement of objects in the acoustic images. If objects are moving, the locations of the pixels of the objects vary. In this case, therefore, averaging pixel-by-pixel can cause the blurring of the resulting images [13].

In this paper, we propose an acoustic image model to predict the changing pixel coordinates under the assumption that the imaging sonar is rotated in the yaw direction, which is the frequent motion for underwater object investigation [14]. On the basis of these models, we develop a speckle noise reduction algorithm by using the Kalman filter (KF) [15]. In the proposed algorithm, the coordinates of each pixel are tracked; thus, the predicted acoustic image can be derived. Using the predicted image and a new measured image, the estimated acoustic image is calculated. These processes are repeated, and the noise-reduced acoustic images are obtained.

The performance of the proposed algorithm is verified by an experiment conducted in an indoor water tank. Target objects are located at the bottom of the water tank, and their acoustic images are obtained using forward-looking imaging sonar. While rotating the imaging sonar along its yaw axis, we measured a series of acoustic image frame, and we applied the proposed algorithm to these image frames. By comparing the raw and processed acoustic image frames obtained using the proposed algorithm, the performance of the proposed algorithm is evaluated.

II. Geometry of Acoustic Image

A. Definition of Sonar Coordinate

In a spherical coordinate system, the coordinate of a given position can be denoted as $\mathbf{p}_s = [r\ \alpha\ \beta]^T$. As shown in Fig. 1, the distance between the origin O and $\mathbf{p}_s$ is denoted as r, and the elevation and azimuth angles are given by α and β, respectively [16]. The coordinate system of the forward-looking imaging sonar, which is called the sonar coordinate system, can be treated as a two-dimensional polar coordinate system [16], [17]. Accordingly, $\mathbf{p}_s$ is projected onto the sonar coordinate as shown in Fig. 1. In this projection, α is disregarded; thus, so the sonar coordinate is given by $\mathbf{p}_p = [r\ \beta]^T$.

B. Relationship between Sonar and Pixel Coordinates of Acoustic Image

The acoustic image can be defined as an $M \times N$ matrix as follows:

$$\mathbf{S} = \begin{bmatrix} s_{11} & s_{12} & \cdots & s_{1N} \\ s_{21} & s_{22} & \cdots & s_{2N} \\ \vdots & \vdots & \ddots & \vdots \\ s_{M1} & s_{M2} & \cdots & s_{MN} \end{bmatrix}, \tag{1}$$

where M and N are the vertical and horizontal resolutions, respectively, of the acoustic image. A pixel value whose coordinate is i and j is denoted as s_{ij} [18].

978-0-933957-43-5 ©2015 MTS

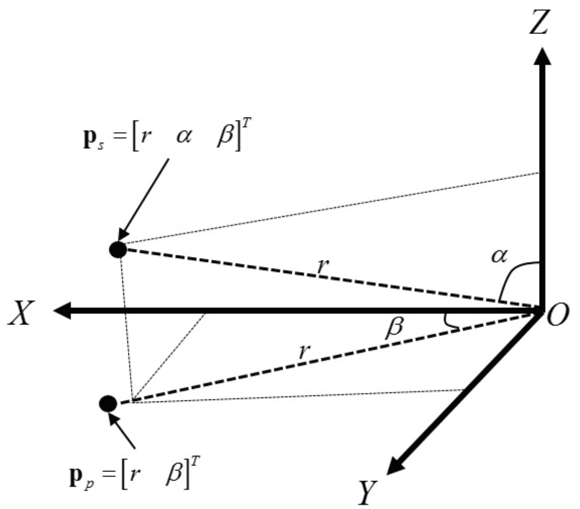

Fig. 1. Acoustic image coordinate of forward-looking imaging sonar.

The position $\mathbf{p}_p$ on the sonar coordinate is mapped to the discrete pixel value. To discuss the mechanism of mapping, we must specify the field of view and range of the imaging sonar, as shown in Fig. 2. The field of view is defined as the lower and upper bounds of the azimuth angle, which are β_{min} and β_{max}, respectively. The range is defined by the minimum and maximum distances, which are denoted as r_{min} and r_{max}, respectively. The area defined by the parameters can be observed by the imaging sonar. On the basis of these definitions, we define the followings:

$$\epsilon_\beta = \frac{\beta_{max} - \beta_{min}}{N} \tag{2}$$

and

$$\epsilon_r = \frac{r_{max} - r_{min}}{M}, \tag{3}$$

where ϵ_β and ϵ_r are the resolutions of the field of view and the range, respectively.

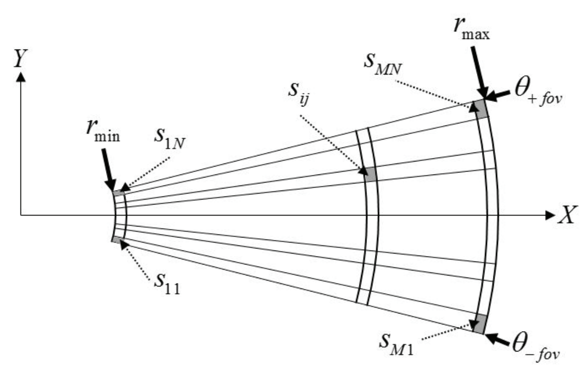

Fig. 2. Relationship between sonar and pixel coordinates.

When the sonar coordinate r and β are given, there exists a pixel s_{ij} that corresponds to these coordinate only if the point given by the sonar coordinates is located within the observable area defined by the field of view and the range. That is, the indices of s_{ij} must satisfy the following conditions: $1 \leq i \leq M$ and $1 \leq j \leq N$. Otherwise, the point given by the sonar coordinates is outside of the observable area, and no pixel corresponding to the coordinates exists. The sonar coordinates can be converted to the pixel indices as follows:

$$i = f_r(r) = \left\lfloor \frac{r - r_{min}}{\epsilon_r} \right\rfloor + 1 \tag{4}$$

and

$$j = f_\beta(\beta) = \left\lfloor \frac{\beta - \beta_{min}}{\epsilon_\beta} \right\rfloor + 1 \tag{5}$$

where $\lfloor x \rfloor$ denotes the nearest integer to x. Conversely, the indices of the pixel are converted to sonar coordinates by the following equations:

$$r = g_r(i) = r_{min} + \epsilon_r (i - 1), \tag{6}$$

and

$$\beta = g_\beta(j) = \beta_{min} + \epsilon_\theta (j - 1) \tag{7}$$

for $1 \leq i \leq M$ and $1 \leq j \leq N$.

III. Modeling of Successive Acoustic Images

A. Model of Pixel Coordinate Change

Sonar imaging can be performed underwater using the following motions: sway, surge, heave, roll, pitch, and yaw [19]. In this paper, we consider only yaw and assume that no other types of motion occur. Yaw involves rotating the aperture of the forward-looking imaging sonar to the left or right, that is, inducing rotation along the Z-axis. Yaw is particularly important for underwater surveying [14]. The forward-looking imaging sonar can be fixed on an autonomous underwater robot (AUV). During investigation, the position, roll, and pitch angles of the AUV can be fixed by its position-keeping control to stabilize the AUV [19]. To search and investigate objects of interest, only the yaw angle of the AUV is changed.

Suppose that the forward-looking imaging sonar yaws during one sampling interval. In this situation, the sonar coordinates are changed as follows:

$$r(t) = r(t-1) \tag{8}$$
$$\beta(t) = \beta(t-1) + \Delta\beta(t), \tag{9}$$

where $r(t)$ and $\beta(t)$ indicate the sonar coordinates at time t. $\Delta\beta(t)$ is the change in the yaw angle during one sampling interval from $t-1$ to t, as shown in Fig. 3. Additionally, we write the pixel value at time t as $s_{ij}(t)$. Its sonar coordinates can be calculated as follows:

$$r(t) = g_r(i) \tag{10}$$
$$\beta(t) = g_\beta(j). \tag{11}$$

According to Equations (8) and (9), we derive the past sonar coordinates at $t-1$ as follows:

$$r(t-1) = r(t) \tag{12}$$
$$\beta(t-1) = \beta(t) - \Delta\beta(t). \tag{13}$$

Using $r(t-1)$ and $\beta(t-1)$, we calculate the indices as follows:

$$i_p = f_r(r(t-1)) \tag{14}$$
$$j_p = f_\beta(\beta(t-1)), \tag{15}$$

where i_p and j_p are the pixel indices of the past sonar coordinates $r(t-1)$ and $\beta(t-1)$. Finally, we obtain the following relationship:

$$s_{ij}(t) = s_{i_p j_p}(t-1). \tag{16}$$

This result enables us to predict the pixels of the acoustic image at time t using the pixel values of the acoustic image at $t-1$ and the change in the yaw angle between $t-1$ and t. As mentioned in Section II, this equation is only applicable when $1 \leq i_p \leq M$ and $1 \leq j_p \leq N$. If these conditions are not satisfied, there is no way to predict $s_{ij}(t)$, because its corresponding pixel in the past acoustic image does not appear within the the observable area of the forward-looking imaging sonar.

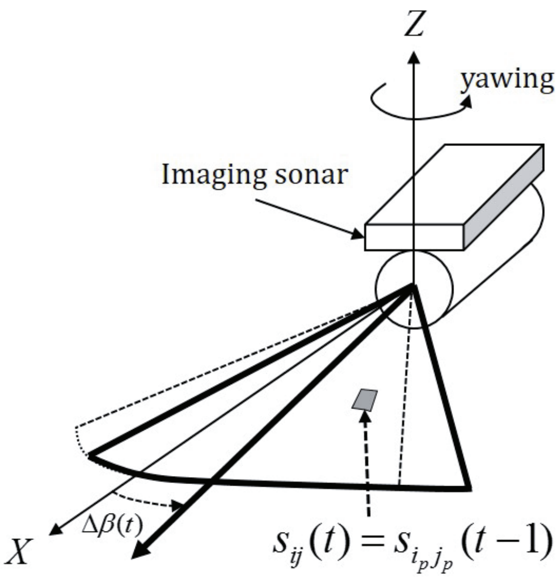

Fig. 3. Pixel coordinate transformation during yaw motion.

B. Model of Noisy Acoustic Image Pixels

Generally, the acoustic image is corrupted by the speckle noise; thus, the measured acoustic image pixel r_{ij} can be modeled as [6]

$$r_{ij}(t) = s_{ij}(t) \times n_{ij}(t), \tag{17}$$

where $n_{ij}(t)$ is the speckle noise. Equation (17) is in nonlinear form; therefore, it cannot be directly applied to the KF, because the KF is a linear estimation algorithm. By applying the natural logarithm to Equation (17), we obtain [20]

$$\begin{aligned} \ln\left(r_{ij}(t)\right) &= \ln\left(s_{ij}(t) \times n_{ij}(t)\right) && (18) \\ &= \ln\left(s_{ij}(t)\right) + \ln\left(n_{ij}(t)\right). && (19) \end{aligned}$$

Therefore, we can write the following measurement equation including additive noise:

$$y_{ij}(t) = x_{ij}(t) + v_{ij}(t), \tag{20}$$

where $y_{ij}(t) = \ln\left(r_{ij}(t)\right)$, $x_{ij}(t) = \ln\left(s_{ij}(t)\right)$, and $v_{ij}(t) = \ln\left(n_{ij}(t)\right)$.

IV. Proposed Algorithm

State-space (SS) equations can represent dynamic systems [15]. SS equations are composed of the system and measurement equations. In this section, we develop the process and measurement equations for a series of acoustic images. The state of the SS equations is defined as the pixels of the acoustic images, and they can be estimated by applying the KF.

A. Kalman Filter

The SS equations a linear time-invariant system are defined as [15]

$$\begin{aligned} \mathbf{x}(t) &= \mathbf{A}\mathbf{x}(t-1) + \mathbf{B}\mathbf{u}(t) + \mathbf{w}(t) && (21) \\ \mathbf{y}(t) &= \mathbf{C}\mathbf{x}(t) + \mathbf{v}(t), && (22) \end{aligned}$$

where $\mathbf{x}(t)$ and $\mathbf{y}(t)$ are the state and measurement vectors. $\mathbf{A}$, $\mathbf{B}$, and $\mathbf{C}$ are the system, input, and measurement matrices of the SS equations. $\mathbf{w}(t)$ and $\mathbf{v}(t)$ are the system and measurement noises, respectively. When the noises are zero-mean white Gaussian noise, the KF can be used to estimate the optimal state vector of the SS equations [15]. With initial conditions $\hat{\mathbf{x}}^+(0)$ and $\mathbf{P}^+(0)$, the time-update formulas of the KF are given by [15]

$$\begin{aligned} \hat{\mathbf{x}}^-(t) &= \mathbf{A}\hat{\mathbf{x}}^+(t-1) + \mathbf{B}\mathbf{u}(t) && (23) \\ \mathbf{P}^-(t) &= \mathbf{A}\mathbf{P}^+(t-1)\mathbf{A}^T + \mathbf{Q}(t), && (24) \end{aligned}$$

for $t = 1, 2, \cdots$. Here, $\hat{\mathbf{x}}^+(t-1)$ is the estimated state vector at $t-1$, and $\hat{\mathbf{x}}^-(t)$ is the predicted state vector at t. $\mathbf{P}^+(t-1)$ and $\mathbf{P}^-(t)$ are the estimation and prediction of the estimation error covariance matrix at $t-1$ and t, respectively. $\mathbf{Q}(t)$ is the covariance matrix of the system noise vector. The measurement update formulas of the KF are given by [15]

$$\begin{aligned} \mathbf{e}(t) &= \mathbf{y}(t) - \mathbf{C}\hat{\mathbf{x}}^-(t) && (25) \\ \mathbf{K}(t) &= \mathbf{P}^-(t)\mathbf{C}^T\left(\mathbf{C}\mathbf{P}^-(t)\mathbf{C}^T + \mathbf{R}(t)\right)^{-1} && (26) \\ \hat{\mathbf{x}}^+(t) &= \hat{\mathbf{x}}^+(t) + \mathbf{K}(t)\mathbf{e}(t) && (27) \\ \mathbf{P}^+(t) &= \left(\mathbf{I} - \mathbf{K}(t)\mathbf{C}\right)\mathbf{P}^-(t), && (28) \end{aligned}$$

where $\mathbf{e}(t)$ is the estimation error vector, and $\mathbf{K}(t)$ is the Kalman gain. $\mathbf{R}(t)$ is the measurement noise covariance matrix. $\mathbf{I}$ is the identity matrix. The time and measurement updates of the KF are recursively repeated, and the estimated state vector converges to the optimal value [15].

B. State-space Equations of Acoustic Image Pixels

For the SS equations of acoustic image pixels, we define the states as the logarithm of $s_{ij}(t)$, i.e., $x_{ij}(t)$. Therefore, we can directly define Equation (20) as the measurement equation.

Now, we discuss the system equation of the SS equations. According to Equation (16), one of the past pixels at $t-1$ can be substituted for a current pixel at t if the pixel is within the observed area of the imaging sonar. Otherwise, the current pixel can not be predicted using the past pixel values. To deal with these complex situations, we propose the following system equation:

$$x_{ij}(t) = x_{ij}(t-1) + u_{ij}(t) + w_{ij}(t), \tag{29}$$

where $u_{ij}(t)$ is treated as a *force* modifying $x_{ij}(t-1)$, and $w_{ij}(t)$ is the system noise added in the pixel. To define $u_{ij}(t)$, we apply the natural logarithm function to Equation (16), obtaining:

$$\ln\left(s_{ij}(t)\right) = \ln\left(s_{i_p j_p}(t-1)\right). \tag{30}$$

Equation (30) can be rewritten as

$$x_{ij}(t) = x_{i_p j_p}(t-1), \tag{31}$$

and is applicable when $1 \leq i_p \leq M$ and $1 \leq j_p \leq N$. Otherwise, we set $x_{ij}(t)$ as zero, because there is no information to determine $x_{ij}(t)$. Consequently, we can define $u_{ij}(t)$ as

$$u_{ij}(t) = \begin{cases} x_{i_p j_p}(t-1) - x_{ij}(t-1), \\ \qquad \text{if } 1 \leq i_p \leq M \text{ and } 1 \leq j_p \leq N \\ -x_{ij}(t-1), \\ \qquad otherwise. \end{cases} \tag{32}$$

C. Proposed Noise Reduction Algorithm

The purpose of the noise reduction algorithm is to estimate $s_{ij}(t)$ on the basis of the noisy measurements. The strategy for the proposed algorithm is shown in Fig. 4. The proposed algorithm has three stages: derivation of $u_{ij}(t)$, time update, and measurement update using the KF.

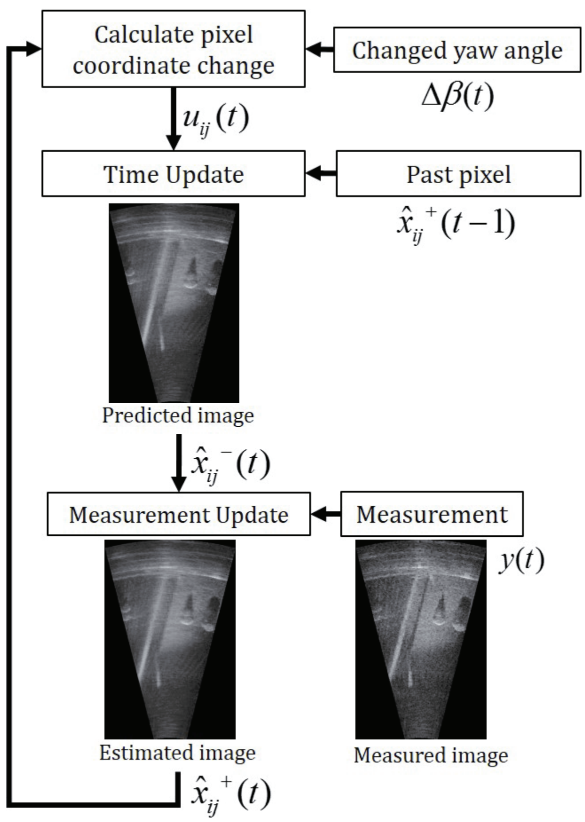

Fig. 4. Proposed strategy for acoustic image enhancement.

Before applying the proposed algorithm, the initial values $\hat{x}_{ij}^{+}(0)$ and $p_{ij}^{+}(0)$ must be defined. At the first stage, the change in yaw angle, $\Delta\beta(t)$, is measured. The indices of the past pixel that correspond to the current pixel can be calculated as follows:

$$i_p = f_r(r(t)) \tag{33}$$
$$j_p = f_\beta(\beta(t) + \Delta\beta(t)), \tag{34}$$

where $r(t) = g_r(i)$ and $\beta(t) = g_\beta(j)$. Then, $u_{ij}(t)$ can be derived as

$$u_{ij}(t) = \begin{cases} \hat{x}_{i_p j_p}^{+}(t-1) - \hat{x}_{ij}^{+}(t-1), \\ \qquad \text{if } 1 \leq i_p \leq M \text{ and } 1 \leq j_p \leq N \\ -\hat{x}_{ij}^{+}(t-1), \\ \qquad otherwise. \end{cases} \tag{35}$$

At the second stage, the time-update of the KF is executed as follows:

$$\hat{x}_{ij}^{-}(t) = \hat{x}_{ij}^{+}(t-1) + u_{ij}(t) \tag{36}$$
$$p_{ij}^{-}(t) = p_{ij}^{+}(t-1) + q_{ij}(t), \tag{37}$$

where $q_{ij}(t)$ is the system noise variance. When $1 \leq i_p \leq M$ and $1 \leq j_p \leq N$, $q_{ij}(t)$ is set to a moderated value. Otherwise, $q_{ij}(t)$ must be set to a large positive value because $\hat{x}_{ij}^{-}(t)$ has high uncertainty.

At the third stage, the pixel value is obtained by the imaging sonar. By taking the natural logarithm of the measured pixel values, we obtain $y_{ij}(t)$. Next, the estimation error is calculated as follows:

$$e_{ij}(t) = y_{ij}(t) - \hat{x}_{ij}^{-}(t). \tag{38}$$

Then, the measurement update is performed using the following equations:

$$g_{ij}(t) = p_{ij}^{-}(t)\left(p_{ij}^{-}(t) + r_{ij}(t)\right)^{-1} \tag{39}$$
$$\hat{x}_{ij}^{+}(t) = \hat{x}_{ij}^{-}(t) + g_{ij}(t)e_{ij}(t) \tag{40}$$
$$p_{ij}^{+}(t) = \left(1 - g_{ij}(t)\right)p_{ij}^{-}(t), \tag{41}$$

where $r_{ij}(t)$ is the measurement noise variance. Finally, the estimated pixel can be derived by taking the exponential function of $\hat{x}_{ij}^{+}(t)$. In consequence, the noise-reduced acoustic image at time t, i.e., $\hat{s}_{ij}(t)$, is given by

$$\hat{\mathbf{S}} = \begin{bmatrix} \hat{s}_{11} & \hat{s}_{12} & \cdots & \hat{s}_{1N} \\ \hat{s}_{21} & \hat{s}_{22} & \cdots & \hat{s}_{2N} \\ \vdots & \vdots & \ddots & \vdots \\ \hat{s}_{M1} & \hat{s}_{M2} & \cdots & \hat{s}_{MN} \end{bmatrix}, \tag{42}$$

where $\hat{s}_{ij}(t) = \exp\left(\hat{x}_{ij}^{+}(t)\right)$. These processes are iteratively executed for each individual pixel.

V. Results

A. Settings

The experiment is conducted in an indoor water tank, as shown in Fig. 5. Three kinds of objects – conical, cylindrical, and spherical in shape, as shown in Fig. 6 – are located at the bottom of the water tank. We equip an rotator to the forward-looking imaging sonar so that the yaw angle of the imaging sonar can be easily adjusted. The forward-looking imaging sonar is installed on the top of the left side wall of the water tank. In our experiment, r_{min} and r_{max} are set to 0.838 and 3.338 m, respectively. The field of view of the forward-looking imaging sonar is 29°, so β_{min} and β_{max} are -14.5° and +14.5°, respectively. We set the forward-looking imaging sonar to identification mode; consequently, the dimensions of the raw acoustic image obtained by the imaging sonar are 512×96.

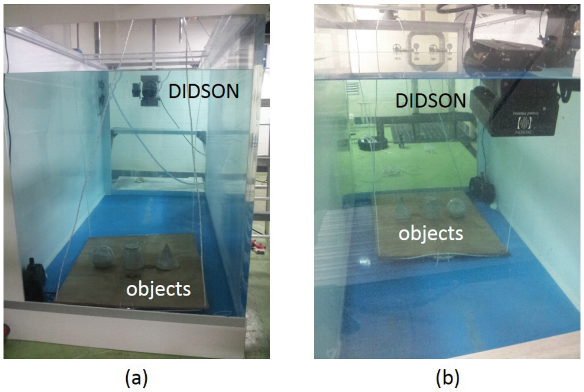

Fig. 5. Photographs of indoor water tank and experimental settings: (a) front view, (b) rear view.

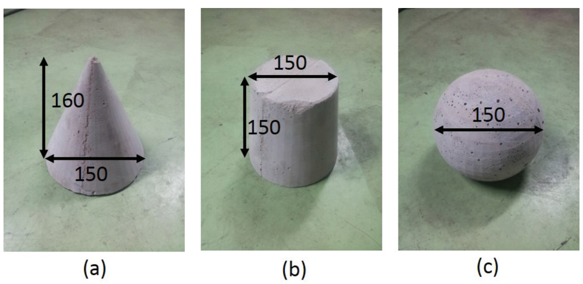

Fig. 6. Photographs of objects used for experiment (unit: mm): (a) conical object, (b) cylindrical object, (c) spherical object.

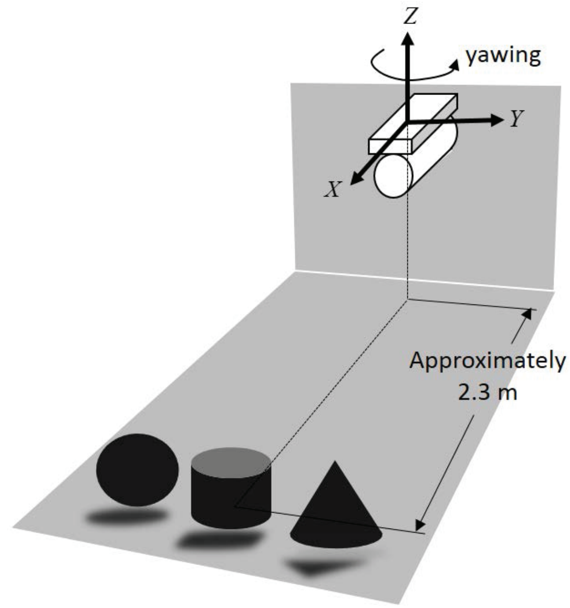

Fig. 7. Experimental settings.

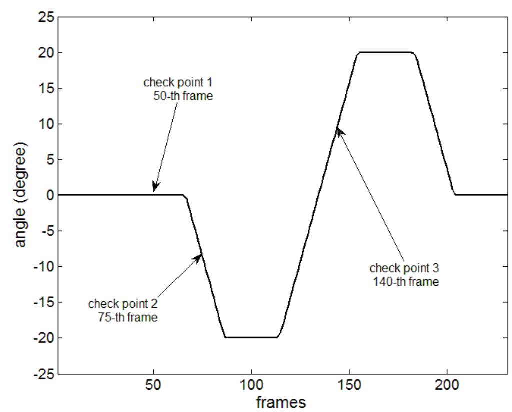

Fig. 8. Variation of yaw angle.

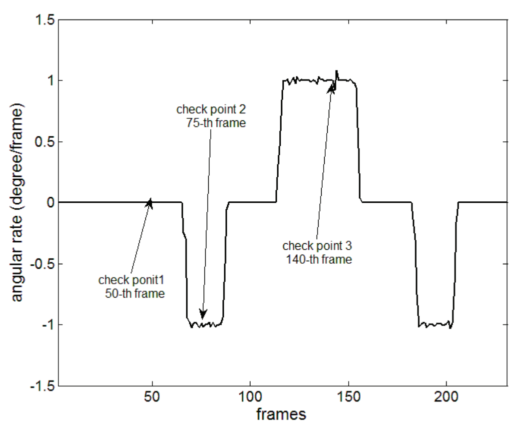

Fig. 9. Variation of yaw angular rate over frames.

While yawing the forward-looking imaging sonar, we measure a series of acoustic image frames. We define the forward direction of the imaging sonar as the positive direction of the X-axis, as shown in Fig. 7. The instant yaw angle of the imaging sonar is the angle between the X-axis and the instant direction of the imaging sonar. The yaw angle of the imaging sonar and its angular rate while acoustic images are measured are graphed in Figs. 8 and 9, respectively. We specify three check points – at 50, 75, and 140 frames – to evaluate the performance of the proposed algorithm.

B. Performance of Noise Reduction

The proposed algorithm is applied to the series of acoustic images. For the proposed algorithm, $r_{ij}(t)$ is set to 0.1. However, q_{ij} is dynamically specified. Under the condition of $1 \le i_p \le M$ and $1 \le j_p \le N$, q_{ij} is set to 0.01. Otherwise, q_{ij} is set to 10. The initial values of the estimated pixels are assigned to the pixel values of the first acoustic image frame. The initial value of the estimation error variance is set to 1.

The raw and processed acoustic images obtained using the proposed algorithm at check point 1, 2, and 3 are shown in Figs. 10, 11, and 12, respectively. These frame-by-frame comparisons indicate that the noise in the acoustic images is slightly decreased compared to the raw acoustic images. However, it seems that there is no significant improvement due to the algorithm. This is because the proposed algorithm is not a conventional spatial-domain filtering algorithm but rather a recursive algorithm that works in the time-domain. To reveal the true effect of the proposed algorithm, the raw and processed acoustic images must be compared with respect to the time-domain.

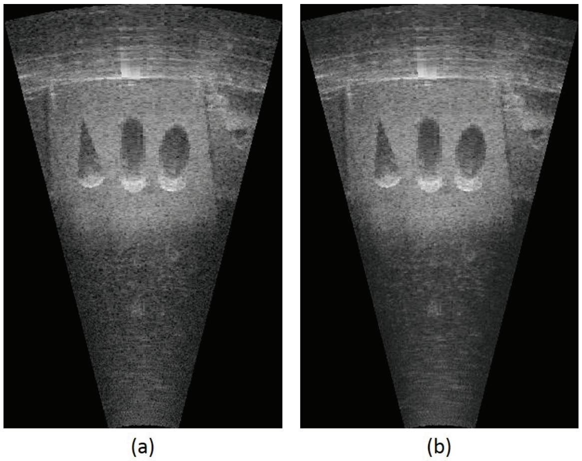

Fig. 10. Comparison between the raw image and processed image at check point 1: (a) raw image, (b) processed image.

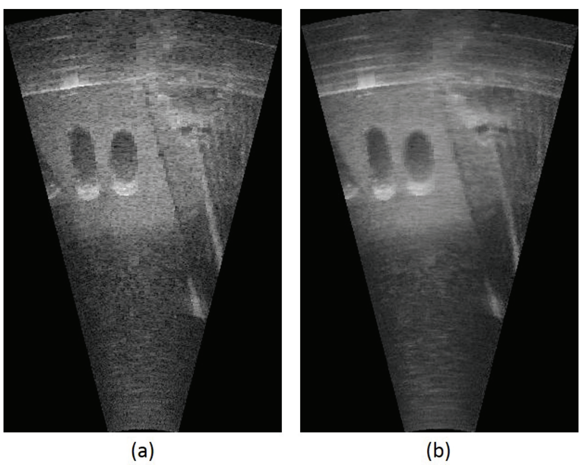

Fig. 11. Comparison between the raw image and processed image at check point 2: (a) raw image, (b) processed image.

To verify the performance of the proposed algorithm over time, we define the difference image as follow:

$$\mathbf{D}(t) = \begin{bmatrix} d_{11}(t) & d_{12}(t) & \cdots & d_{1N}(t) \\ d_{21}(t) & d_{22}(t) & \cdots & d_{2N}(t) \\ \vdots & \vdots & \ddots & \vdots \\ d_{M1}(t) & d_{M2}(t) & \cdots & d_{MN}(t) \end{bmatrix}, \quad (43)$$

where $d_{ij}(t) = |\hat{s}_{ij}(t) - \hat{s}_{ij}(t-1)|$. The pixel values of the difference images at check point 1, 2, and 3 are represented in Figs. 13, 14, and 15, respectively. At check point 1, the forward-looking imaging sonar is fixed; thus, there is no pixel coordinate change. Therefore, the pixel values of the difference image in this situation are ideally expected to be close to zero, but because of the speckle noise, the pixel values rather high, as shown in Fig. 13 (a). On the other hand, the pixels of the processed difference image have low values that are close to zero; this is also shown in Fig. 13 (b). These results indicate that the proposed algorithm can effectively eliminate the speckle noise.

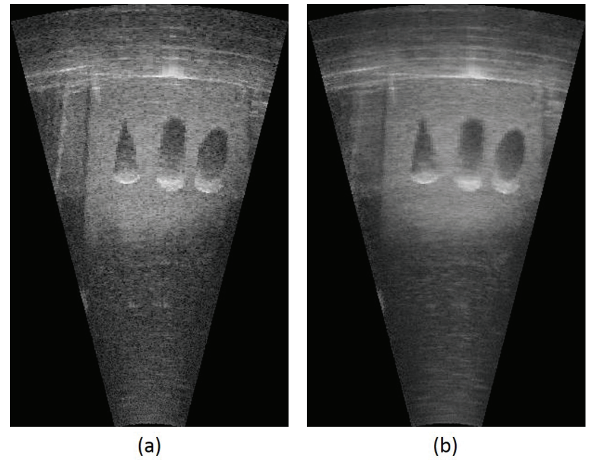

Fig. 12. Comparison between the raw image and processed image at check point 3: (a) raw image, (b) processed image.

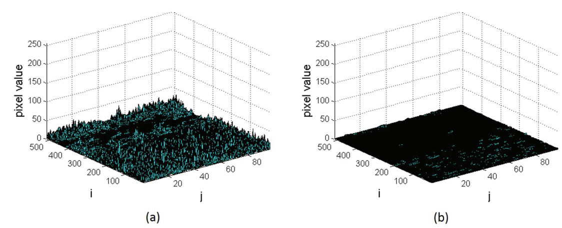

Fig. 13. Graph of raw and processed difference images at check point 1: (a) raw image, (b) processed image.

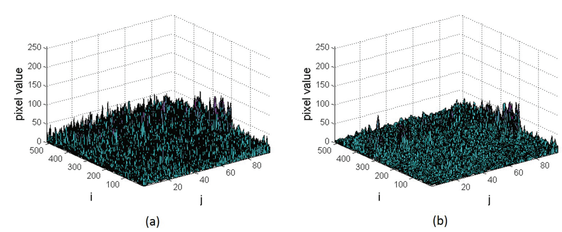

Fig. 14. Graph of raw and processed difference images at check point 2: (a) raw image, (b) processed image.

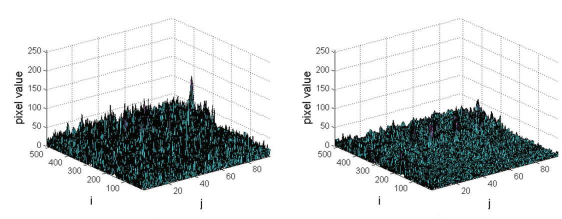

Fig. 15. Graph of raw and processed difference images at check point 3: (a) raw image, (b) processed image.

At check points 2 and 3, the forward-looking imaging sonar is rotated; therefore, the pixel values of the difference images are higher than those at check point 1, as shown in Figs. 14 (a) and 15 (a). This is because the rotation causes a change in pixel coordinates. Although the pixels are changed by the rotation, the difference images processed by the proposed algorithm have lower pixel values than the raw difference images, as shown in Figs. 14 (b) and 15 (b). These results indicate that the proposed algorithm can used to reduce the speckle noise over time, even if the forward-looking imaging sonar is yawing.

C. Feasibility of Pixel Tracking

As shown in Figs. 11 (b) and 12 (b), the proposed algorithm can be used to derive the processed image without image distortion such as blurring even if the forward-looking imaging sonar is yawing. Therefore, the proposed algorithm can be used to accurately track the change of pixel coordinates on the basis of the prediction model.

To illustrate this ability of the proposed algorithm, we apply the proposed algorithm in the same manner as in the previous experiment but altering the value of the change in yawing angle $\Delta\beta(t)$. In this experiment, we set $\Delta\beta(t)$ to zero for every iteration. This means that the pixel coordinate prediction executed in the time update is not used; only the measurement update is performed.

The results of this experiment are shown in Fig. 16. At check point 1, the processed image – as shown in Fig. 16 (a) – appears identical to the processed image in Fig. 10 (b). This is the expected result because there is no change in yaw angle until check point 1. However, the processed image at check point 2 is blurred, as shown in Fig. 16 (b). This is because the changed yaw angle is not used for the algorithm, even if the imaging sonar is rotating at check point 2. Therefore, the image prediction of the proposed algorithm is essential for treating the rotation. If the image prediction is not applied, the noise reduction algorithm in the time domain can be only used for the acoustic images obtained using fixed imaging sonar.

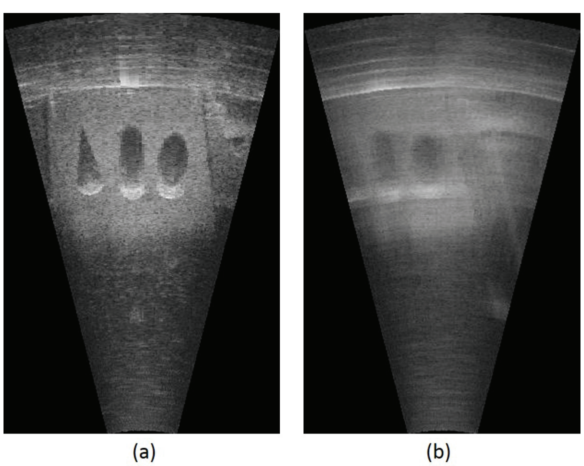

Fig. 16. Processed acoustic images without prediction of pixel coordinate change.

VI. Conclusion

In this paper, we propose a speckle noise reduction algorithm for sonar imaging. A series of acoustic image frames similar to optical video images is obtained using the imaging sonar. The proposed algorithm is based on the KF, which is a recursive estimation algorithm in the time domain; therefore, the variation of pixels of the successive acoustic images can be treated in real time. For the proposed algorithm, the pixel coordinate change is modeled to track the variation of pixels when the imaging sonar is yawing. Consequently, the proposed algorithm can be applied in underwater surveying that requires the yaw motion to search and investigate surrounding objects.

Acknowledgment

This research was a part of the project titled “Gyeongbuk Sea Grant Program,” funded by the Ministry of Oceans and Fisheries, Korea. This research was supported by the ministry of science, ICT and future planning, Korea, under the ”ICT Consilience Creative Program” (IITP-2015-R0346-15-1007) supervised by the institute for information & communications technology promotion.

References

[1] J. Yuh, ”Design and Control of Autonomous Underwater Robots: A Survey,” *Autonomous Robots*, vol. 8, no. 1, pp. 7-24, 2000.

[2] J. S. Jaffe, ”Computer modeling and the design of optimal underwater imaging systems,” *IEEE J. of Oceanic Eng.*, vol, 15, no. 2, pp. 101-111, 1990.

[3] R. Schettini and S. Corchs, “Underwater Image Processing: State of the Art of Restoration and Image Enhancement Methods,” *EURASIP J. on Advances in Sig. Processing*, doi: 10.1155/2010/746052, 2010.

[4] E. Belcher, W. Hanot, and J. Burch, “Dual-frequency identification sonar (DIDSON),” *Proc. of Int. Symp. on Underwater Technology*, 2002, pp. 187-192.

[5] F. M. Caimi, D. M. Kocak, F. Dalgleish, and J. Watson, “Underwater imaging and optics: Recent advances,” *OCEANS*, 2008, pp. 1-9.

[6] F. Chaillan, C. Faschini, and P. Courmontagne, “Speckle noise reduction in sas imagery,” *Signal Process*, vol. 87, no. 4, pp. 762-781, 2007.

[7] M. V. Sarode and P. R. Deshmukh, “Reduction of Speckle Noise and Image Enhancement of Images Using Filtering Techniques,” *Int. J. of Advancements in Technology*, vol. 2, no. 1, pp. 30-38, 2011.

[8] D. Kuan, A. Sawchuk, T. Strand, and P. Chavel, “Adaptive restoration of images with speckle,” *IEEE Trans. on Acoustics, Speech and Signal Processing*, vol. 35, no. 3, pp. 373-383, 1987.

[9] S. Sudha, G. R. Suresh, and R. Sukanesh, “Speckle Noise Reduction in Ultrasound Images by Wavelet Thresholding based on Weighted Variance,” *Int. J. of Computer Theory and Eng.*, vol. 1, no. 1, pp. 7-12, 2009.

[10] E. Belcher and D. C. Lynn, “Acoustic, near-video-quality images for work in turbid water,” *Proc. of Underwater Intervention*, 2000, pp. 187-192.

[11] S. -C. Yu, Z. Teng, and D. -J. Kang, ”Modeling of high-resolution 3d sonar for image recognition,” *Int. J. offshore and Polar Engineering*, vol. 22, no. 3, pp. 1-7, 2012.

[12] J. D. Hamilton, “Time series analysis,” *Princeton University Press*, Princeton, NJ., 1994.

[13] H. Cho and S. -C. Yu, “Real-time sonar image enhancement for AUV-based acoustic vision,” *Ocean Eng.*, vol. 104, pp. 568-579, Aug. 2015.

[14] P. Ridao, M. Carreras, D. Ribas. and R. Garcia, “Visual Inspection of Hydroelectric Dams Using an Autonomous Underwater Vehicle,” *J. of Field Robotics*, vol. 27, no. 6, pp. 759-778, 2010.

[15] S. Haykin, “Adaptive Filter Theory,” *Prentice Hall*, Englewood Cliffs, NJ., 2004.

[16] S. Negahdaripour, “Epipolar Geometry of Opti-Acoustic Stereo Imaging,” *IEEE Trans. on Pattern Analysis and Machine Intelligence*, vol. 29, no. 10, pp. 1776-1788, Oct. 2007.

[17] K. Kim, N. Neretti, and N. Intrator, “Mosaicing of acoustic camera images,” *IEE Proceedings - Radar, Sonar and Navigation*, vol. 152, no. 4, pp. 263-270, Aug. 2005.

[18] B. P. Murphy, “Image Processing Techniques for Acoustic Images,” *Naval Postgraduate School*, 1991.

[19] J. Pyo, H. Joe, and S. -C. Yu, “Development of the AUV System for Precision Visual Data Collection,” *Int. Offshore and Polar Eng. Conf.*, 2013, pp. 337-342.

[20] G. Padmavathi, P. Subashini, M. Kumar, and S. Thakur, “Comparison of Filters used for Underwater Image Pre-Processing,” *Int. J. of Computer Science and Network Security*, vol. 10, no. 1, pp. 58-65, 2010.